J. Marine Sci. Appl. (2017) 16: 298 -304
DOI: 10.1007/s11804-017-1422-x

Numerical Investigation of Hydrodynamic Flow Over an AUV Moving in the Water-surface Vicinity Considering the Laminar-turbulent Transition

Mahmoud Salari* **and Amin Rava**

Department of Mechanical Engineering, Imam Hossein University, Tehran 1655853548, Iran

Abstract: Nowadays, Autonomous Underwater Vehicles (AUVs) are frequently used for exploring the oceans. The hydrodynamics of AUVs moving in the vicinity of the water surface are significantly different at higher depths. In this paper, the hydrodynamic coefficients of an AUV in non-dimensional depths of 0.75, 1, 1.5, 2, and 4D are obtained for movement close to the free-surface. Reynolds Averaged Navier Stokes Equations (RANS) are discretized using the finite volume approach and the water-surface effects modeled using the Volume of Fraction (VOF) method. As the operating speeds of AUVs are usually low, the boundary layer over them is not fully laminar or fully turbulent, so the effect of boundary layer transition from laminar to turbulent flow was considered in the simulations. Two different turbulence/transition models were used: 1) a full-turbulence model, the k-ε model, and 2) a turbulence/transition model, Menter's Transition-SST model. The results show that the Menter's Transition-SST model has a better consistency with experimental results. In addition, the wave-making effects of these bodies are studied at different immersion depths in the sea-surface vicinity or at finite depths. It is observed that the relevant pitch moments and lift coefficients are non-zero for these axi-symmetric bodies when they move close to the sea-surface. This is not expected for greater depths.

Keywords: autonomous underwater vehicles, sea surface effects, computational fluid dynamics, hydrodynamics, laminar to turbulent transition

Article ID: 1671-9433(2017)03-0298-07

1 Introduction

Ocean exploration and an understanding of the underwater world are of utmost importance. To explore the deep seas, it is a necessity to design suitable appliances and equipment to negate the need for human presence in the undersea. To this end, a variety of unmanned submarines have been developed. Autonomous Underwater Vehicles (AUVs) or simply Underwater Vehicles (UWVs) are used in many applications such as measurement and sea-probing, exploration and exploitation of seabed minerals, inspection and maintenance of offshore structures, and anti-submarine warfare (Nematollahi *et al.*, 2015). The operating conditions of AUVs at sea can be categorized into three types; at the sea-surface vicinity, at intermediate depths, and in the vicinity of the sea-floor. The main challenge for the design of underwater vehicles is to match their capabilities with different operating conditions while retaining maneuverability. The wave-making phenomena of the AUVs, while they are moving horizontally near the sea-surface, results in non-zero lift forces and pitch moments, even for axi-symmetric bodies. Due to these effects, providing dynamic stability for AUVs moving close to the sea-surface has great importance and complexity. During its operation, an AUV will experience frequent sea-surface effects, especially when receiving data from GPS navigation. For this reason, an assessment of the hydrodynamic loadings acting on subsea bodies close to the sea-surface and at different speeds is important. To evaluate the hydrodynamic performance of immersed moving AUVs, fluid-flow governing equations need to be accurately solved. Practically, as the forces and momentum in these equations are expressed in terms of hydrodynamic coefficients, these coefficients should be obtained before making a prototype. There are some experimental, semi-experimental, and numerical methods which can be used to compute the hydrodynamic coefficients of moving underwater bodies, especially for axi-symmetric bodies moving far from the sea-surface. However, when an immersed moving vehicle reaches the sea-surface vicinity, the coefficients calculated for high or intermediate depths are no longer valid and cannot be used to assess maneuverability and stability in these conditions. In this case, the dynamics of the body's motion is affected by the free-surface and some free-surface waves are induced. Prediction of the hydrodynamic coefficients of an AUV as a function of immersion depth is of utmost importance in engineering.

The overall resistance of AUVs moving near the sea-surface consists of two components: viscous resistance including friction and pressure, and wave-making resistance (Vorus *et al.*, 2010). Recent advances in numerical techniques have provided affordable solutions for calculating hydrodynamic coefficients. Finite volume methods based on Computational Fluid Dynamics (CFD) are effective for simulating the effect of the water-surface on underwater bodies. In the field of identifying submarine hydrodynamic features at greater depths and far from the sea-surface, a lot of

Received date: 30-Dec-2016
Accepted date: 17-Apr-2017
***Corresponding author Email:** msalari@ihu.ac.ir; m.salari@gmail.com

studies have been carried out by researchers in the form of laboratory tests and numerical methods. For example, Zhao *et al.* (2009) and Shao *et al.* (2013) numerically solved the steady flow around vertical and oblique cylinders. Laboratory experiments on the structure of flow around a cylinder, the coefficients of forces acting on it, and its effect on the water-surface have been carried out by Malavasi and Guadagnini (2007) considering various flow conditions and heights from a channel bottom.

Significant work has also been performed to predict the hydrodynamic coefficients of AUVs, for example studies by Phillips *et al.* (2010) Tang *et al.* (2009) Lee *et al.* (2011) and Ross *et al.* (2004). In comparison to the many studies that have been carried out on the hydrodynamic coefficients of immersed objects far from the free-surface conditions, few researchers have focused on two-phase flow and the free-surface effects on the hydrodynamic forces and moments of such bodies. Due to the complexity and nonlinearity of two-phase flow and the free-surface problem, only a few researchers, such as Hajmohammadi *et al.* (2014a; 2014b) have used analytical methods to solve their governing equations. Among the numerical work carried out to predict hydrodynamic forces on immersed bodies due to surface waves, the work of Wiley (1994) can be noted. Malik *et al.* (2013) also used CFD to calculate wave forces in both the time and frequency domains. In the above studies, the assumptions of potential flow, a slender body, and finite motion have been used and the accuracy of the results depends on the validity of these assumptions. A few researchers such as Jagadeesh *et al.* (2009; 2010) and Nematollahi *et al.* (2015) used the Reynolds averaged Navier Stokes, RANS equations to study the effect of a free-surface on the hydrodynamic coefficients of an axi-symmetric underwater body. All used full-turbulence models to analyze the hydrodynamics of these bodies. However, their results show considerable differences compared with experimental data, especially at low immersion depths.

As these bodies move at a relative lower speed underwater, the boundary layer regime over their surfaces may experience a transition from laminar to turbulent flow, and some regions might be exposed to laminar or transitional flows. Therefore, in this study, numerical results of CFD simulations around an underwater body in depth in vicinity of the free surface were obtained using two numerical turbulence/transition models. The full-turbulence model of *k-ε* and the four-equation transition model of Menter's Transition-SST (Menter *et al.*, 2006), were compared with experimental data. Accounting for the effects of the transitional process from laminar to turbulent flow on these bodies is the novelty feature of this research.

2 Problem definition

In this study, the hydrodynamic characteristics of an axi-symmetric body moving near the water surface, considering the effects of the laminar to turbulent transition process in the boundary layers is investigated numerically. The study was carried over the speed range 0.4 to 1.4 m/s and at immersion depths from 0.75 to 4 times the diameter of the body. Simulations were performed based on solving the RANS equations and using two turbulence/transition models: 1) the full-turbulence model of *k-ε* and 2) the four-equation turbulence/transition model of Menter's Transition-SST. Two transport equations in the second model were developed to predict the location of the transition onset from a laminar to turbulent regime, and the lengths of these transitions. This model also can simulate the turbulent regions of boundary layers as reported by Menter *et al.* (2006). Modeling of the laminar/turbulent transition is very important for the correct prediction of hydrodynamic characteristics of fluid flow as the transition substantially influences skin friction and therefore energy loss (Taghavi *et al.*, 2006; 2008; 2009).

The hydrodynamic coefficients obtained from the simulations were then compared with the experimental results of Jagadeesh *et al.* (2009). A schematic of an axi-symmetric body is shown in Figure 1, where *h* is the distance from the water-surface and *D* is the maximum diameter of the body. Dimensionless parameters used in the simulation includes the Reynolds number $Re=\rho UV^{1/3}/\mu$ ranging from 1.05×10^5 − 3.67×10^5), immersion factor $H=h/D$ ranging from 0.75 − 4, and Froude number, *Fr*.

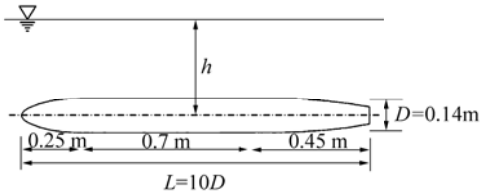

Fig. 1 Schematic of a symmetrical AUV body

3 Governing equations and numerical simulation

For the hydrodynamic modeling of an AUV in the vicinity of a free-surface, the continuity, momentum, and a RANS based turbulence/transition model were solved for both air and water phases using the VOF approach. In the RANS equation, the Reynolds stresses, $\overline{u_i u_j}$, were determined using two different turbulence models; a full-turbulence model and a turbulence/transition model.

The continuity and RANS equations are as follows:

$$\frac{\partial U_j}{\partial x_j}=0 \tag{1}$$

$$\frac{\partial U_i}{\partial t}+\left(U_j\frac{\partial U_i}{\partial x_j}+\frac{\partial \overline{u_i u_j}}{\partial x_j}\right)=-\frac{\partial P}{\partial x_j}+\frac{1}{Re}\nabla^2 U_i \tag{2}$$

The transport equations of the *k-ε* full-turbulence model need to be solved to obtain the Reynolds stresses, as follows:

$$\frac{\partial k}{\partial t}+\left(U_j-\frac{1}{\sigma_k}\frac{\partial \nu_t}{\partial x_j}\right)\frac{\partial k}{\partial x_j}=\frac{1}{R_k}\nabla^2 k+G-\varepsilon \tag{3}$$

$$\frac{\partial \varepsilon}{\partial t}+\left(U_j-\frac{1}{\sigma_\varepsilon}\frac{\partial \nu_t}{\partial x_j}\right)\frac{\partial \varepsilon}{\partial x_j}=\frac{1}{R_\varepsilon}\nabla^2\varepsilon+\frac{\varepsilon}{k}\left(C_{\varepsilon 1}G-C_{\varepsilon 2}\varepsilon G\right) \quad (4)$$

In the above equations, U_i represents the main components of velocity, p is the pressure, and G is the level of kinetic energy production. Other details of the model can be seen in Jagadeesh *et al.* (2010). The Menter's Transition-SST turbulence/transition model was developed by Menter *et al.* (2006) to model the laminar, transitional, and turbulence features in transitional flows. It can predict the location of transition onset based on empirical correlations and can also provide an estimation of the length of the transition region. It should be noted, that the development of RANS-based transition/turbulence models for predicting transitional flows has been of more interest since the year 2000. A literature review on transitional fluid-flow simulations can be found in Taghavi *et al.* (2006; 2008; 2009).

The Menter's Transition-SST turbulence/transition model is a powerful tool for modeling transitional flows. This model has four transport equations: two for predicting the transition onset and evaluating intermittency within the transitional region, and the other two for modeling turbulence characteristics using the *k*-*ω*-SST turbulence model. The *k*-*ω*-SST model benefits both the *k*-*ω* and *k*-*ε* turbulence models and was in good agreement with the experimental results. The first equation of the Menter's Transition-SST turbulence/transition model is the intermittency transport equation, used for evaluating the laminar/turbulence quantities within the transition region. The transport equation for the intermittency, γ, is as follows:

$$\frac{\partial(\rho\gamma)}{\partial t}+\frac{\partial(\rho U_j\gamma)}{\partial x_j}=P_{\gamma 1}-E_{\gamma 1}+P_{\gamma 2}-E_{\gamma 2}+\frac{\partial}{\partial x_j}\left[\left(\mu+\frac{\mu_t}{\sigma_\gamma}\right)\frac{\partial \gamma}{\partial x_j}\right] \quad (5)$$

The second transport equation transports a scalar variable called the transition's Reynolds number of momentum thickness, $\widetilde{Re}_{\theta t}$, within the flow field. It has been formulated to predict the transition onset in transitional flows. It is as follows:

$$\frac{\partial \rho u_j \widetilde{Re}_{\theta t}}{\partial x_j}=P_{\theta t}+\frac{\partial}{\partial x_j}\left[\sigma_{\theta t}\left(\mu+\mu_t\right)\frac{\partial \widetilde{Re}_{\theta t}}{\partial x_j}\right] \quad (6)$$

The third and fourth transport equations of this turbulence/transition model are same as the equations of the *k*-*ω*-SST turbulence model.

To solve the transport equations, a commercial CFD code (Fluent 16.0) was used. This is based on the finite volume method. The SIMPLE algorithm was also used for coupling the pressure and velocity fields within the domain. A second-order upwind was used for discretizing the momentum and turbulence/transition models.

4 Multiphase modeling

The main issues for modeling in this present work were the computational simulation of the water free-surface and capture of the relevant surface-wave propagation. Two common methods are proposed in the literature to perform these simulations; the marker-and-cell (MAC) and the VOF. Both have the ability for nonlinear simulation and wave-breaking. The MAC method calculates the free-surface by recording the momentum of fluid particles. This method requires the location of each particle therefore; it often occupies a large amount of storage space and needs considerable computing time (Tome and McKee *et al*., 1994). In contrast, the VOF method is more consistent with many engineering applications, including the calculation of free-surface flow (Shen *et al*., 2004; Zhao *et al*., 2010). In the present work, the VOF model was used to calculate surface waves made by the underwater body moving near the water free-surface. The governing principals of the VOF method, developed by Hirt and Nichols (1981) are based on the conservation of mass and momentum for two or more non-miscible fluids. It has been used to detect the interface between fluid phases. In this method, the fluid phase in a computational cell is modeled by the volume fraction of each fluid, such that their fractions are between zero and one, and their sum is equal to one.

Mathematical equations to measure the volume fraction α_i can be expressed as follows:

$$\frac{\partial \alpha_i}{\partial t}+\boldsymbol{U}\times\nabla\alpha_i=0 \quad (7)$$

$$\sum_{i=1}^{2}\alpha_i=1 \quad (8)$$

$$\rho=\alpha_1\rho_1+\left(1-\alpha_1\right)\rho_2 \quad (9)$$

where ρ_1 and ρ_2 are the densities of two different types of immiscible fluids.

5 The computational domain and boundary conditions

For the numerical simulation, a 3D computational domain of $39D\times10D\times5D$ was used according to Jagadeesh *et al.*, (2009). The computational domain is shown in Figure 2. A schematic of the immersion depths of the body is also shown. At the entrance to the domain, the inlet pressure boundary condition was set by the two parameters of speed and free-surface height. The boundary condition of the output pressure at the outlet was characterized by determining the height of the free-surface. The upper and lower boundaries of the domain were set as a slipping wall. The side boundary surfaces were adjusted to a symmetrical plane. To discretizing the computational domain a structured mesh was used (Fig. 3). To better capture the flow-field quantities close to the free-surface, smaller cells were used at the water/air boundary. To ensure that the numerical results remained independent of

the number of cells within the computational domain, and to select adequate cell sizes for the smaller cells nearest to the body's surface, the number and size of cells were changed for body speeds of 1.4 m/s and depths of h/D = 0.75. Table 1 shows number of cells that can be achieved in the domain corresponding to the range of y^+. Figure 4 shows the drag or resistance coefficient dependency on the number of cells in the computational domain. According to these results, for a domain with over 0.8 million cells, the drag/resistance coefficient does not change significantly. Fig. 5 shows the variations in y^+ for the selected case of *E* in Table 1.

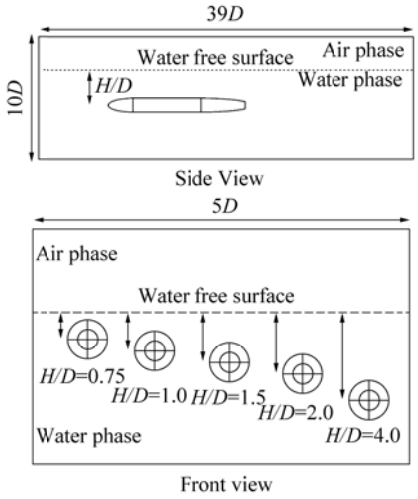

Fig. 2 Schematic of the computational domain

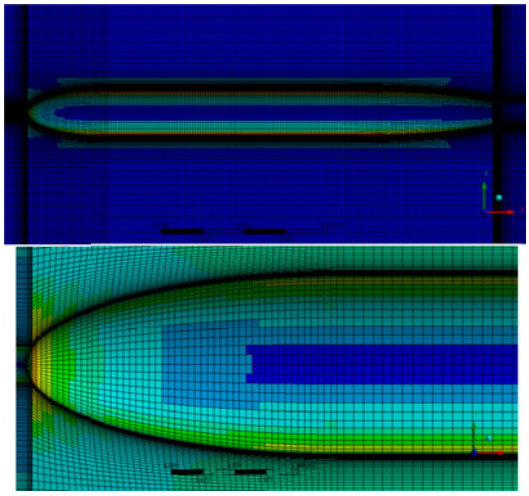

Fig. 3 Schematic of the structured grid

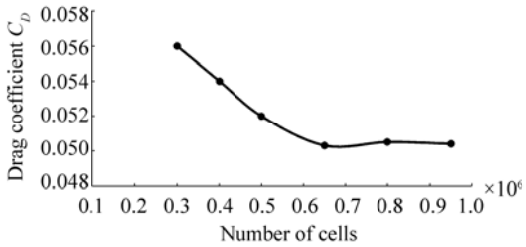

Fig. 4 Study of the grid independency

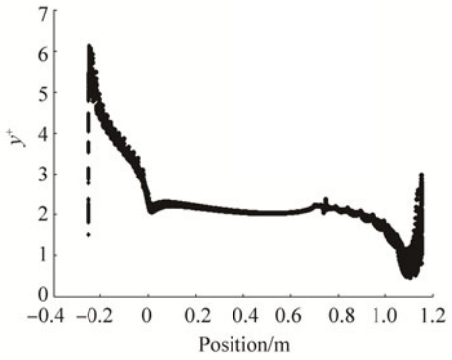

Fig. 5 Variations in y^+ along the body for the case of *E* of Table 1 and [*H* = 0.75*D*, 1.4 m/s]

Table 1 Different cases for domain meshing

Case	y^+ range	Number of cells ($\times 10^6$)
A	$130 < y^+ < 140$	0.3
B	$100 < y^+ < 120$	0.4
C	$50 < y^+ < 90$	0.5
D	$22 < y^+ < 30$	0.65
E	$12 < y^+ < 20$	0.8
F	$5 < y^+ < 10$	0.95

6 Results and discussion

The hydrodynamic characteristics of an underwater vehicle, with a body of revolution subjected to the effects of a water free-surface, were investigated numerically. Hydrodynamic coefficients were determined over the speed range 0.4 to 1.4 m/s ($Re = 3.67\times10^5$) and at different depths of H ($0.75D - 4.0D$). For the simulation, two different turbulence/transition models were used and the results compared with the experimental data obtained by Jagadeesh *et al.*(2009, 2010). In this study, the results are presented for different immersion depths, according to the dimensionless number $Fr = U/\sqrt{gL}$ by changing the speed. Fig. 6 shows the drag coefficient C_D variation with the immersion depth H as the Froude number varied. It can be seen that the numerical results from Menter's Transition-SST model (dashed line) show good consistency with the experimental data from Jagadeedh *et al.* (2009) while the results obtained from the *k-ε* turbulence model (solid line) deviates from the experimental data, especially at lower *H/D* ratios. Also, for most cases, the drag coefficients obtained from the *k-ε* fully turbulent model are higher than those from experiments. This could be due to this turbulence model considering a fully-turbulent boundary layer over the whole body, while under actual conditions, a transitional boundary layer occurs over the body surface and the front of the body surface experiences a laminar boundary layer. In must be noted, that the local skin friction coefficient of a turbulent boundary layer is higher than that of a laminar boundary layer under the same Reynolds number conditions. As expected, the Transition-SST model, which captures the transition from laminar to turbulent flow, follows the experiments. However, at all depths, the overall drag coefficient reduced with increasing Froude number

(equivalent to increasing the speed). Also, it is clearly evident that for a fixed Froude number, when the immersion depth H decreases, the overall drag coefficient increases.

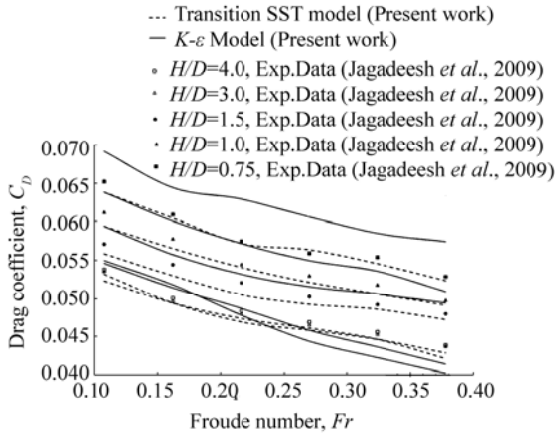

Fig. 6 Variation in drag coefficient versus Froude number at different depths

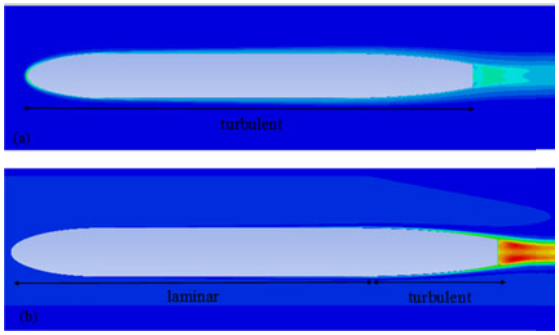

Fig. 7 Contours of turbulent kinetic energy; a) k-ε turbulence model and b) Menter's SST-Transient model

Fig. 8 Variations in intermittency over the body surface, computed using Menter's SST-Transition model (laminar region, blue; turbulent region, red)

The intermittency in the Menter's SST-Transition model, Eq. (5), indicates turbulent or laminar features within the fluid flow field. It has a maximum value of one within the fully-turbulent region and a minimum value of zero in the fully-laminar region. In the transition region the intermittency varies from zero to one.

The basic difference between the full-turbulence k-ε model and Menter's SST-Transition model is the determination of the transitional region in the latter model. In the k-ε model, the whole boundary layer around the body is assumed to be turbulent, while in the transition/turbulence Menter model, the laminar, transitional and turbulent boundary layers are distinguishable. The turbulent kinetic energy contours and the intermittency factor are shown in Figs. 7 and 8, respectively. Fig. 7(a) shows the turbulent kinetic energy of the k-ε model at Fr = 0.11. As mentioned, in this turbulence model, the whole boundary layer region is assumed to be turbulent, which is different in reality. Fig. 7(b) shows the turbulent kinetic energy computed by Menter's SST-Transition model at Fr = 0.11. Fig. 7(b) shows that the SST-Transition model has enough capability to capture the transitional boundary layers, from laminar to turbulent. In Fig. 8, the intermittency coefficient over the body surface, obtained from the SST-transition model, is shown for the same flow conditions as used for the results in Fig. 7.

By reducing the immersion depth of the underwater body, its interaction with the water-surface increases, therefore, an additional term, the wave-making resistance, should be added to the overall drag of the body, similar to that obtained for deep-sea conditions. In hydrodynamic studies of AUVs, the wave-making drag/resistance is an important parameter. The wave-making resistance is defined as the difference between the total body drag while moving in the water-surface vicinity and that under deep-sea conditions, where there is not any interaction between the body and the water-surface. For this comparison, the same speed and angle of attack conditions are considered.

An analysis and classification of resistance forces in marine applications is shown in Fig. 9, which provides different levels of resistance forces (Bertram, 2012; Rawson 2001). A basic and well-known classification for overall resisting force in marine engineering is the sum of wave resistance, pressure resistance, and friction resistance, $R_T = R_W + R_{PV} + R_F$. According to this definition, the pressure resistance is as follows: $R_P = R_W + R_{PV}$.

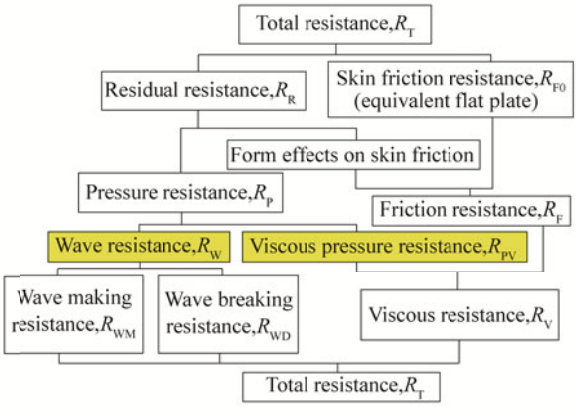

Fig. 9 The components of total resistance RT in marine applications (Rawson, 2001)

As expected, the reason for the increase in total resistance or drag coefficient with reducing immersion depth is the increase in the wave-making resistance component on the underwater body. However, for greater immersion depths, the wave-making resistance partially decreases or fully removed. The results show that for an immersion depth $H > 3D$ the wave-making resistance is negligible. Fig. 10 shows the effect of the free-surface on the lift coefficient, C_L, when the

underwater body moves in the water-surface vicinity. This figure shows that when the underwater body moves in a depth $H > 3D$, due to the symmetry condition of the flow fields around the body, the lateral force tends to be very small and negligible. As the immersion depth decreases, the flow field around the underwater body will be asymmetric and lateral forces and pitch moments will be created while the body moves horizontally. For these AUV configurations, the lateral force is positive and upward, so it lifts the body up toward the water-surface.

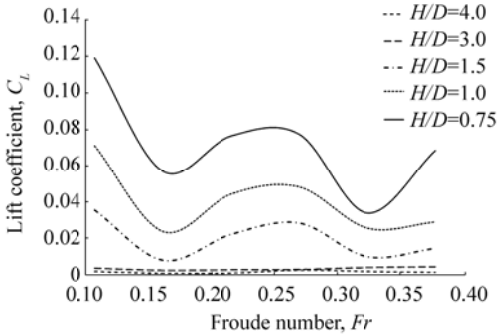

Fig. 10 Variation in lift coefficient, C_L, versus Froude number, Fr, at different depths

The effects of underwater body motion on the water-surface profiles at different speeds can be also obtained. Fig. 11 shows the water free-surface or wave profiles at the speed of u = 1.4 m/s for various depths. It is evident that by decreasing the immersion depth, the relevant wave height increases. It was also observed that for $H > 3$, no considerable wave was generated on the water-surface.

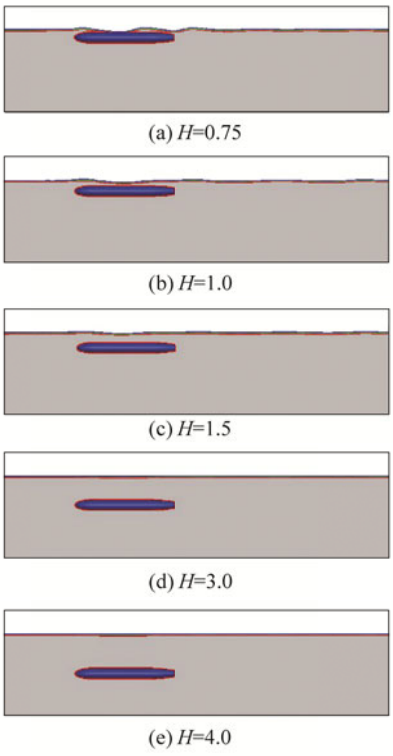

Fig. 11 Water free-surface profile characteristics versus immersion depth, u=1.4 m/s and Fr=0.38

Fig. 12 shows the effect of speed variation of the underwater body on wave profiles for the depth H=0.75D. It can be observed that with increasing body speed, the generated wave height also increases. The wavelength also increases and is approximately equal to the length of underwater body. At low speeds, the wavelength is lower and hence the wave frequency on body increases.

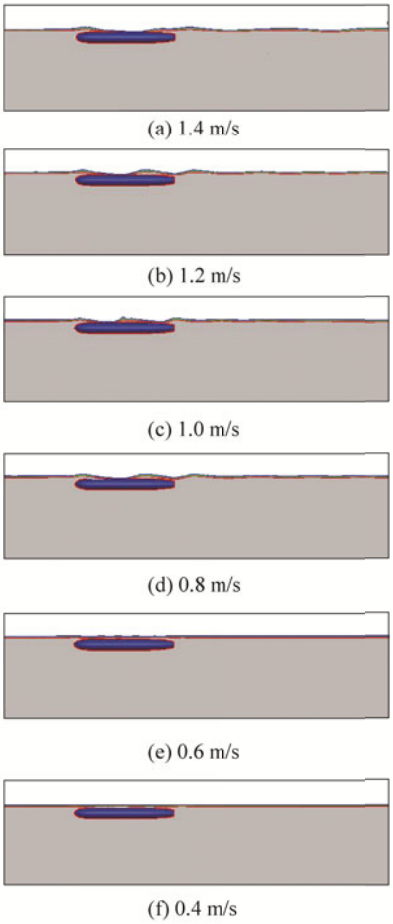

Fig. 12 Water free-surface profile due to underwater body motion at H=0.75D under different speeds

7 Conclusions

In this paper, a set of numerical simulations of two-phase flow were conducted to evaluate the effects of moving in the vicinity of a water free-surface on the hydrodynamic coefficients of an AUV. The results were compared with the experimental results of Jagadeesh *et al.* (2009) and showed good agreement. This study was performed at different depths from H = 0.75D to H = 4D, and with different Froude numbers, $Fr = U/\sqrt{gL}$ from 0.11 to 0.38. The results show that the effect of a water free-surface on the resistance or drag coefficient of underwater bodies is dependent on the immersion depth and speed. In water free-surface vicinity, due to wave-making resistance, an increase in the underwater body drag or resistance coefficients can be observed. This is

in comparison to the conditions where the body moves at greater depths, greater than $H = 3D$. According to these results, when an underwater body moves close to the surface, the flow-field around the body is not symmetric about its horizontal mid-plan compared to that at greater depths.

References

Bertram V, 2012. *Practical ship hydrodynamics*. Elsevier.

Hajmohammadi MR, Nourazar SS, 2014a. On the insertion of a thin gas layer in micro cylindrical Couette flows involving power-law liquids. *International Journal of Heat and Mass Transfer*, **75**(31), 97-108.
DOI: 10.1016/j.ijheatmasstransfer.2014.03.065

Hajmohammadi MR, Nourazar SS, Campo A, 2014b. Analytical solution for two-phase flow between two rotating cylinders filled with power law liquid and a micro layer of gas. *Journal of Mechanical Science Technology*, **28**(5), 1849-1854.
DOI: 10.1007/s12206-014-0332-y

Hirt CW, Nichols BD, 1981. Volume of fluid (VOF) method for the dynamics of free boundaries. *Journal of computational physics*. **39**(1), 201-25.
DOI: 10.1016/0021-9991(81)90145-5

Jagadeesh P, Murali K, 2010. RANS predictions of free surface effects on axisymmetric underwater body. *Engineering Applications of Computational Fluid Mechanics*, **4**(2), 301-313.
DOI: 10.1080/19942060.2010.11015318

Jagadeesh P, Murali K, Idichandy VG, 2009. Experimental investigation of hydrodynamic force coefficients over AUV hull form. *Journal of Ocean Engineering*, **36**(1), 113-118.
DOI: 10.1016/j.oceaneng.2008.11.008

Lee SK, Joung TH, Cheo SJ, Jang TS, Lee JH, 2011. Evaluation of the added mass for a spheroid-type unmanned underwater vehicle by vertical planar motion mechanism test. *International Journal of Naval Architecture and Ocean Engineering*, **3**(3), 174-180.
DOI: 10.2478/IJNAOE-2013-0060

Malavasi S, Guadagnini A, 2007. Interactions between a rectangular cylinder and a free-surface flow. *Journal of Fluids and Structures*, **23**(8), 1137-1148.
DOI: 10.1016/j.jfluidstructs.2007.04.002

Malik, SA, Pan G, Liu YA, 2013. Numerical simulations for the prediction of wave forces on underwater vehicle using 3D panel method code. *Research Journal of Applied Sciences, Engineering and Technology*, **5**(21), 5012-5021.

Menter FR, Langtry RB, Likki SR, Suzen YB, Huang PG, Völker S, 2006. A correlation-based transition model using local variables-part I: model formulation. *Journal of Turbomachinery*, **128**(3), 413-422.
DOI: 10.1115/1.2184352

Nematollahi A, Dadvand A, Dawoodian M, 2015. An axisymmetric underwater vehicle-free surface interaction: a numerical study. *Journal of Ocean Engineering*, **96**, 205-214.
DOI: 10.1016/j.oceaneng.2014.12.028

Phillips A, Turnock SR, Furlong M, 2010. The use of computational fluid dynamics to aid cost-effective hydrodynamic design of autonomous underwater vehicles. *Proceedings of the Institution of Mechanical Engineers, Part M: Journal of Engineering for Maritime Environment,* **224**(4), 239-254.
DOI: 10.1243/14750902JEME199

Rawson KJ, 2001. *Basic ship theory*. Vol. 1, Butterworth-Heinemann.

Ross A, Fossen TI, Johansen TA, 2004. Identification of underwater vehicle hydrodynamic coefficients using free decay tests. *IFAC Conference on Control Applications in Marine Systems, Ancona*, Italy.

Shao WY, Zhang YP, Zhu DZ, Zhang TQ, 2013. Drag force on a free surface-piercing yawed circular cylinder in steady flow. *Journal of Fluids and Structures*, **43**, 145-163.
DOI: 10.1016/j.jfluidstructs.2013.09.007

Shen YM, Ng CO, Zheng YH, 2004. Simulation of wave propagation over a submerged bar using the VOF method with a two-equation k–ε turbulence modeling. *Journal of Ocean Engineering*, **31**(1), 87-95.
DOI: 10.1016/S0029-8018(03)00111-2

Taghavi ZR, Salari M, 2006. Prediction of Boundary Layer Transition at High Freestream Turbulence Conditions Using a Physical Model. *Aerospace Mechanics Journal*, **2**(2), 85-95.

Taghavi ZR, Salari M, Etemadi M, 2008. Prediction of laminar, transitional and turbulent flow regimes, based on three-equation k-ω turbulence model. *Aeronautical Journal*, **112**(1134), 469-476.
DOI: 10.1017/S0001924000002438

Taghavi ZR, Salari M, Kolaei A, 2009. Prediction of boundary layer transition based on modeling of laminar fluctuations using RANS approach. *Chinese Journal of Aeronautics*, **22**(2), 113-120.
DOI: 10.1016/S1000-9361(08)60076-X

Tang S, Ura T, Nakatani T, Thornton B, Jiang T, 2009. Estimation of the hydrodynamic coefficients of the complex-shaped autonomous underwater vehicle TUNA-SAND. *Journal of Marine Science and Technology*, **14**(3), 373-386
DOI: 10.1007/s00773-009-0055-4

Tome MF, McKee S, 1994. GENSMAC: A computational marker and cell method for free surface flows in general domains. *Journal of Computational Physics*, **110**(1), 171-186.
DOI: 10.1006/jcph.1994.1013

Vorus WS, Paulling JR, 2010. *The Principles of Naval Architecture Series*.

Willy CJ, 1994. *Attitude control of an underwater vehicle subjected to waves*. Ph.D thesis, Massachusetts Institute of Technology and Woods Hole Oceanographic Institute.

Zhao M, Cheng L, Zhou T, 2009. Direct numerical simulation of three-dimensional flow past a yawed circular cylinder of infinite length. *Journal of Fluids and Structures*, **25**(5), 831-847.
DOI: 10.1016/j.jfluidstructs.2009.02.004

Zhao XZ, Hu CH, Sun ZC, 2010. Numerical simulation of extreme wave generation using VOF method. *Journal of Hydrodynamics*, *Ser. B*, **22**(4), 466-477.
DOI: 10.1016/S1001-6058(09)60078-0